

14.9 ASSESSMENT OF GPS OCCULTATIONS FOR ATMOSPHERIC PROFILING

G. A. Hajj*, E. R. Kursinski, W. I. Bertiger, L. J. Remans

Jet Propulsion Laboratory
California Institute of Technology
Pasadena, CA 91109

K. R. Hardy

Lockheed Missiles & Space Company, inc.
Palo Alto, CA 94304-1191

1. INTRODUCTION

The concept of utilizing the global positioning system (GPS) signals as a means of sensing the atmosphere, originally suggested by Yunck et al. [1], has been studied in some detail in the literature [2-8]. The idea is to place one or more receivers in low-Earth orbit (LEO) that are continuously tracking the GPS with fields of view extending down to the limb of the Earth. As a GPS satellite is occulting behind the atmosphere as seen from a LEO satellite, the signal traveling through the lowest 70 km of the atmosphere is delayed and bent sufficiently to give accurate refractivity in that region of the atmosphere with a vertical resolution of about 1 km [3]. Assuming hydrostatic equilibrium and the ideal gas law, atmospheric density, temperature and pressure can be derived from refractivity. Generally, sub-Kelvin temperature accuracy appears possible between heights of 10-50 km, and refractivity can generally be obtained to better than 0.3% down to the surface [5]. The presence of appreciable water vapor in the troposphere makes interpretation of refractivity ambiguous. In this region, solving for either temperature or water vapor is generally not possible without ancillary data. Exceptions exist in some climatic regimes such as in polar winter where water vapor contribution is small and temperature accurate to within 1 K is possible down to the surface [4]. Another special case exists in the tropics where the temperature profiles are relatively uniform over large distances and for long periods. Knowledge of the temperature profile there allows one to solve for water vapor.

A satellite in a polar LEO tracking the present 26 GPS satellites with a full view of the Earth's limb will provide over 500 globally distributed occultations daily. The delay and bending induced by the atmosphere on the signal are typically 0.7- 1.6 km and 1-2° at the Earth's surface depending on the humidity level. These decrease exponentially with height with a scale height equal to

the atmospheric density scale height. Larger delay and bending are possible when very sharp refractivity gradients are encountered in the atmosphere.

When proper care is taken to control all the different types of errors that contribute to the retrieval such as receiver thermal noise, clock drifts, multipath, ephemeris errors and ionosphere, the phase measurement will have a sub-millimeter precision [8]. Absolute temperature errors of 0.5 K and less appear to be typical of profiles in the altitude range between 10 and 45 km, and may be as low as 0.1 K in the vicinity of the tropopause consistent with the simulation results of Gorbunov and Sokolovskiy [7].

The effect of water vapor uncertainty on temperature recovery in the lower troposphere and vice versa is discussed in section 2.10 section 3, we examine briefly the residual ionospheric effects on the retrieval and means of minimizing them. In section 4, we present a preliminary analysis of GPS data taken from atop Mauna Kea, Hawaii at 4200 m altitude, looking down below the horizon in an occulting geometry and compare them to simulation based on radiosonde data from Hilo, HI.

2. INTERRELATIONSHIP BETWEEN WATER VAPOR AND TEMPERATURE UNCERTAINTIES

The refractivity is related to the temperature, pressure, and water vapor pressure via

$$N = 77.6 \frac{P}{T} + 3.73 \times 10^{-5} \frac{P_w}{T^2}, \quad (1)$$

where T is in K and P and P_w in mbars. When the water vapor content is significant such as the case in the troposphere, separation between the dry and moist terms is ambiguous. In this case, one can solve for temperature given the water vapor density; alternatively, one can solve for water vapor density given the temperature and pressure. Given a very precise measurement of N , in this section we estimate the uncertainty in temperature (water vapor density) for a given uncertainty in water vapor (temperature and pressure). Based on (1), one can easily relate the

*Corresponding author address: Jet Propulsion Laboratory, 4800 Oak Grove Dr., Pasadena, CA 91109

uncertainty in water vapor to those of temperature and pressure via

$$\frac{\delta P_w}{P_w} = \frac{77.6}{3.73 \times 10^5} \left(\frac{PT}{P_w} \right) \left(\frac{\delta T}{T} - \frac{\delta P}{P} \right) + 2 \frac{\delta T}{T} \quad (2)$$

In deriving (2) we set $\delta N/N$ to zero.

2.1 Temperature Uncertainty Due to Water Vapor

If we take $\delta P_w = 0.5 P_w$, representing a 50% uncertainty in assumed water vapor abundance, then an amount of 0.25 and 0.5 grains of water vapor per kilogram of air results in 1 and 2 K uncertainties respectively. This effect is summarized in the dashed lines of Fig. (1) which is based on annual average climatological data from Peixoto and Oort [9]. In our estimation we ignore the pressure uncertainty based on the fact that it accumulates slowly relative to density uncertainties. The top two curves in the figure indicate the approximate pressure levels at which a 50% uncertainty in water vapor abundance produces 1 and 2 K temperature errors. It is clear from this figure that colder regimes allow these profiles to extend to lower altitudes because of the very strong temperature dependence of the Clausius-Clapeyron behavior of water vapor pressure equilibrium. A specific example of a profile retrieved under high latitude winter conditions is discussed by Kursinski et al. [4]

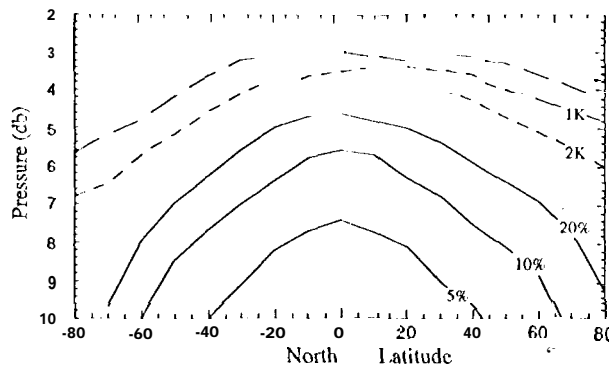


Fig. 1: Temperature uncertainty (K) due to 50% uncertainty of water vapor density (dashed lines), and fractional water vapor density (%) uncertainties due to 2 h' and 7 mb of uncertainties in temperature and surface pressure,

2.2. Water Vapor Uncertainty Due to Temperature and Pressure

Given the pressure and temperature, we now estimate the uncertainty in the retrieved water vapor. In this case pressure error cannot be ignored, but can be related to the temperature error through the hydrostatic equilibrium equation which yields

$$\frac{\delta P(h)}{P(h)} = \frac{\delta P_s}{P_s} + \int_0^h \frac{\delta T}{T} \frac{dh}{H} \quad (3)$$

where P_s and δP_s are surface pressure and pressure error respectively, H is the density scale height, and h is height. Contours representing annual average water vapor profile accuracies of 5, 10 and 20% are shown in Fig. 1 (solid lines). In obtaining these, we assumed a fractional temperature error of 7×10^{-3} (-2° K) and surface pressure error of 7 mb. It is clear that most accurate and vertically extensive profiles will be produced in the tropics where water vapor abundances are greatest. A specific example of a water vapor profile retrieved in the tropics is discussed by Kursinski et al. [3]. A more in depth discussion of how the uncertainties in temperature, pressure and water vapor map into each other is discussed further by Kursinski et al. [8]

3. IONOSPHERIC EFFECT REMOVAL

The Earth's ionosphere extends from roughly 90 km altitude upwards and acts as a lens overlaying the neutral atmosphere. Since signals pass through the ionosphere on their way into and out of the neutral atmosphere below, the effect of the ionosphere must be adequately estimated and removed to produce accurate profiles within the neutral atmosphere. The dispersive nature of the ionosphere, causes signals of different frequencies to travel at different speed. A simple linear combination of the two L-band signals transmitted by the GPS, L1 (1575.42 MHz) and L2 (1227.6 MHz), is commonly used to remove the first-order effect of the ionosphere which is in the range of 1-100 m. The residual ionospheric effects, if left uncalibrated, act as an important source of error that maps into neutral atmospheric profile errors [5].

The dominant residual ionospheric error is due to the splitting of the two signals in the ionosphere, causing the atmosphere to be probed at slightly different heights. Based on the Parameterized Ionospheric Model [10] for the ionosphere, we estimate the amount of separation between the L1 and L2 rays at the tangent point. This is shown in Fig. 2. (left scale) for day- and night-time, solar maximum conditions. During daytime, this ranges from roughly 20 m near the Earth's surface, to about 500 m near 100 km altitude, and is about an order of magnitude smaller during the night. Also shown in Fig. 2 (right scale) is the magnitude of this term as a percentage of the total neutral atmospheric delay, where neutral refractivity is assumed to be exponentially decaying with a constant scale height of 7 km. It is clear from this example, that this error would be a substantial fraction of the total effect at all heights (0.5-7%) for daytime. One can reduce the effect of this term by obtaining a first order estimate of the neutral refractivity profile, and then estimating the ray separation (A) according to the following equation

$$A \approx d_2 \delta_2 - d_1 \delta_1 \quad (4)$$

where d_i, δ_i correspond to the ray asymptote distance and bending to the GPS satellite (Fig. 3). One can then

use the estimated separation and the first order solution of the, neutral atmospheric refractivity to estimate and remove the splitting term. A refined solution of the neutral atmospheric refractivity can be obtained by iterating the procedure a few times until convergence. Fig. 2 shows the difference between the estimated ray separation and the true one for the daytime example. The 0.5-7% error is reduced to -0.0.2% error, which will map to sub-Kelvin-level temperature errors.

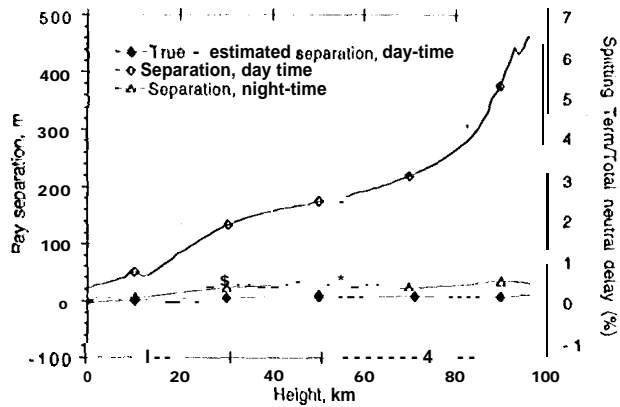


Fig. 2: Modeled day and night ray separation (left scale) and ratio of residual error due to the splitting of signals over the total atmospheric effect (right scale) as a function of tangent height. Calibrated daytime effects are also shown.

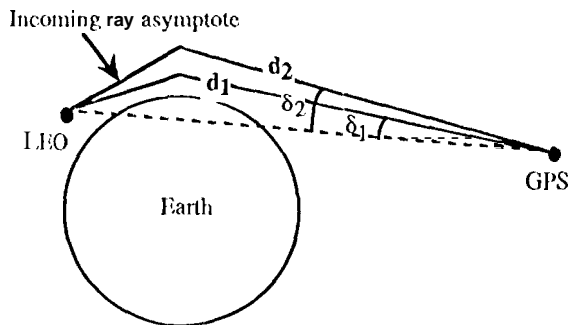


Fig. 3: Pictorial representation of the ray asymptotes and bending angles in an occultation geometry.

4. OCCULTATION FROM ATOP MAUNA KEA

Many of the features of the GPS occultation concept can be tested by replacing the L110 receiver by a ground station on a high mountain tracking GPS down to the horizon. In this section we present very preliminary analysis of data taken from atop Mauna Kea, Hawaii (4200 m altitude) and compare it to a simulation based on radiosonde measurements taken from nearby Hilo, HI.

The Hawaiian islands are in a region characterized by a strong and persistent temperature inversion at the top of the marine boundary layer with height varying from 1 to 4 km. The inversion is characterized by moist air below and warmer and drier air above.

The temperature and dew point profiles obtained from the radiosonde released at 2307 UTC (1307151') on 30 Sept 1993 from Hilo, HI are shown in Fig. 4. The sounding included measurements up to 30 km but only the lowest 10 km is shown in the figure. The sharp increase in temperature and decrease in moisture (dew point), which define the inversion level at the top of the boundary layer, are clearly evident at a height of 1.5 km. There are also several significant changes in the dew point between 5 and 10 km.

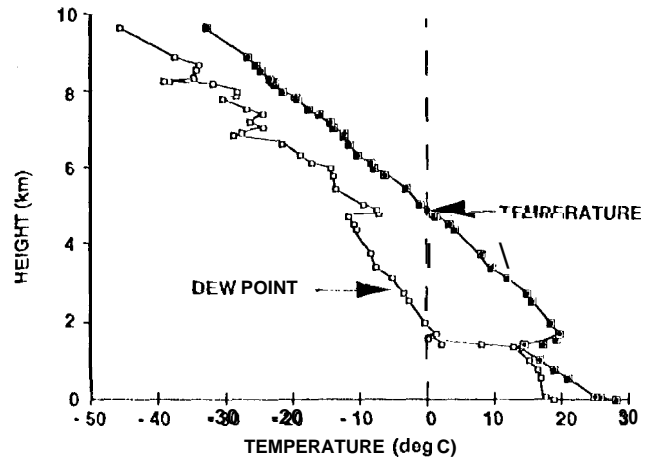


Fig. 4: The temperature and dew point profiles for Hilo, HI 30 Sept 1993. 2307 UTC.

The refractive index profile can be computed from the temperature and moisture profiles. As expected, there is a very large decrease in the refractive index near the inversion; the sharpest gradient amounts to 42 N units over a height of 100 m which greatly exceeds the gradient of about 16 N units per 100 m, for trapping or ducting of radio rays. Thus, in an occultation measurement from the top of Mauna Kea through the atmosphere represented in Fig. 4, complex and multiple ray paths can be expected as the tangent point of the rays approaches 1.5 km, the height of the inversion.

We are in the preliminary state of analyzing the GPS measurements taken at Mauna Kea about two hours after the time of the radiosonde data. Based on this analysis, the atmospheric delay as a function of the satellite elevation is shown in Fig. 5, along with a simulation based on the Hilo radiosonde data. Given that the receiver is at 4200 m altitude, an elevation of -3.7° implies that the signal is bending by about -1.7° . The fact that the data terminate before the simulation could indicate that the receiver lost lock of the signal before it completely disappeared behind the horizon.

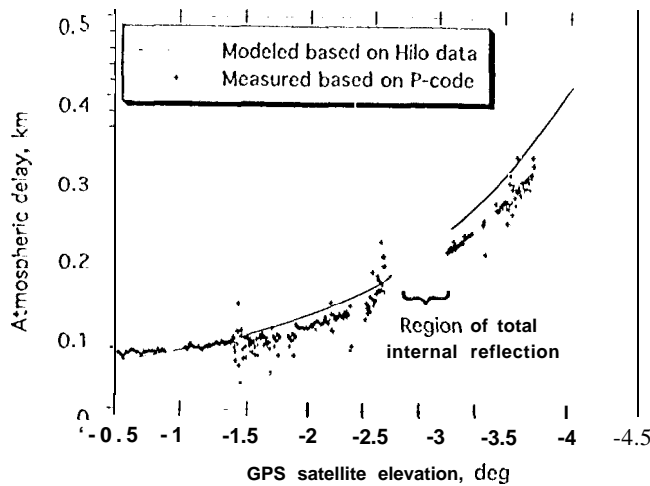


Fig. 5: Atmospheric delay based on GPS measurements taken from Mauna Kea on Oct 1, 1:00 UTC and modeled based on Hilo radiosonde data taken two hours earlier.

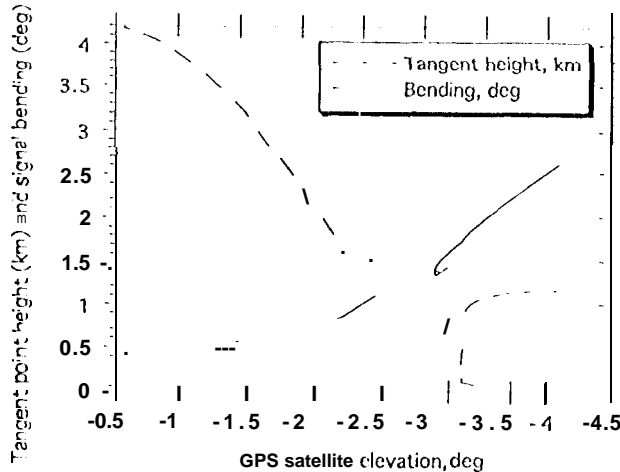


Fig. 6: Simulated GPS signal bending and height of the closest qpr each point as a function of elevation based on the Hilo radiosonde data.

The largest data gap in the measurements, which is in very good agreement with the simulation, occurs when the tangent point of the ray is entering the inversion layer capping the marine boundary layer at -1.5 km. This height can be read from Fig. 6, which shows the simulated tangent height and amount of the signal bending based on the Hilo radiosonde data. The large vertical gradients associated with the boundary layer lead to significant fluctuation in the data during the last 10-20 seconds due to defocusing. This is reflected in the measurements presented in Fig. 5 in the region immediately before the largest data gap. The sharp defocusing of the signal as it descends near the boundary layer can be deduced from Fig. 6 by observing how the tangent height flattens out, namely the ray descends very slowly, while the bending is increasing more rapidly as the satellite is descending. The signal

reappears after about 90 seconds from a broad region in the boundary layer (which is seen from the nearly vertical line at -3.1° elevation of Fig. 6). This would cause a sharp focusing of the received signal, as well as potentially strong scintillation and multipath. The multi-valued functions of the tangent height and bending as a function of elevation (Fig. 6) imply that the signal is arriving at the receiver via two different paths, an effect referred to as atmospheric multipath. The signal's extinction and re-appearance provide a clear and accurate indication of the height of the marine boundary layer and an accurate estimate of the change of refractivity above and below the boundary layer.

The work described in this paper was carried out in part at the Jet Propulsion Laboratory, California Institute of Technology, under contract with the National Aeronautics and Space Administration, and in part under the Lockheed independent research program,

REFERENCES

- [1] Yunck TP, GG Lindal, CH Liu, The role of GPS in precise earth observation, *Proc. of IEEE position location and navigation symp.* Orlando, 1988.
- [2] Hardy KR, DP Hinson, GL Tyler, ER Kursinski, Atmospheric profiles from active space-based radio measurements, *Proc. of the 6th Conference on Satellite Meteorology and Oceanography*, The American Meteorological Society, Boston, 1992.
- [3] Kursinski ER, GA Hajj, KR Hardy, Temperature and moisture profiles from radio occultation measurements, *Proc. of the 8th Symp. on Meteorological Observations and Instrumentation*, pp. J153-J158, The American Meteorological Society, Anaheim, 1993.
- [4] Kursinski ER, GA Hajj, KR Hardy, Atmospheric profiles from radio occultation measurements of GPS Satellites, *Proc. of the International Symp. for Optical Engineering and Photonics in Aerospace Science and Sensing*, paper no. 1935-13, International Soc. for Optical Eng., Orlando, 1993.
- [5] Hardy KR, GA Hajj, ER Kursinski, Accuracies of atmospheric profiles obtained from GPS occultations, *Proc. of the ION-GPS 9.2 Conf.*, Institute of Navigation, Salt Lake City, 1993.
- [6] Yuan JJ, RA Anthes, RH Ware, C Rocken, WD Bonner, MG Bevis, S Businger: Sensing climate change using the GPS, *JGR*, 98:14925-14937, 1993.
- [7] Gorbunov MB and SV Sokolovskiy, Remote sensing of refractivity from space for global observations of atmospheric parameters, Max-Planck-Institut für Meteorologie, Hamburg, Report No. 119, Dec. 1993.
- [8] Kursinski ER et al., Monitoring the Earth's Atmosphere with Radio Occultation Measurements Using GPS, to be submitted to *JGR*, 1994.
- [9] Peixoto JP and AH Oort, *Physics of Climate*, pp. 140 and 281, American Institute of Physics, NY, 1992.
- [10] Daniell RE, WG Whartenby, JD Brown, Parameterized Real-time Ionospheric Specification Model, Version 1.2, Computation Physics, Inc. Newton, MA, 1993.